Magnetic Weyl Semimetal in $K_2Mn_3(AsO_4)_3$ with the Minimum Number of Weyl Points

Simin Nie,[1,*,†] Tatsuki Hashimoto,[2,†] and Fritz B. Prinz[1,2,‡]
[1]*Department of Materials Science and Engineering, Stanford University, Stanford, California 94305, USA*
[2]*Department of Mechanical Engineering, Stanford University, Stanford, California 94305, USA*

(Received 28 September 2021; revised 25 March 2022; accepted 30 March 2022; published 27 April 2022)

The “hydrogen atom” of magnetic Weyl semimetals, with the minimum number of Weyl points, has received growing attention recently due to the possible presence of Weyl-related phenomena. Here, we report a nontrivial electronic structure of the ferromagnetic alluaudite-type compound $K_2Mn_3(AsO_4)_3$. It exhibits only a pair of Weyl points constrained in the z direction by the twofold rotation symmetry, leading to extremely long Fermi arc surface states. In addition, the study of its low-energy effective model results in the discovery of various topological superconducting states, such as the hydrogen atom of a Weyl superconductor. Our Letter provides a feasible platform to explore the intrinsic properties related to Weyl points, and the related device applications.

DOI: 10.1103/PhysRevLett.128.176401

Introduction.—The realization of elementary particles (i.e., Dirac, Weyl, and Majorana fermions) in condensed matter has received growing attention due to high scientific interest and promising applications in novel quantum devices [1–21]. Compared with Dirac and Majorana fermions, Weyl fermions do not need any specific symmetry protection (but the lattice translation symmetry) to guarantee their existence. Weyl semimetals exhibit linear dispersion around discrete doubly degenerate points [termed Weyl points (WPs)], whose low-energy excitation exactly satisfies the Weyl equation of quantum field theory [22]. In momentum space, the WPs with positive and negative chirality can be viewed as the “source” and “drain” points of the “magnetic field” [23], respectively. According to the “no-go theorem” [24], the total chirality in the entire three-dimensional Brillouin zone (BZ) must be zero, i.e., the WPs always appear in pairs of opposite chirality. Therefore, the minimum numbers of WPs in nonmagnetic and magnetic Weyl semimetals are four and two, respectively. This type of Weyl semimetals, called “hydrogen atom” of Weyl semimetals [25], are of great interest due to the simple phenomena related only to WPs, such as large negative magnetoresistance [26–28] and large anomalous Hall conductivity [29–32]. These properties are particularly important for related device designs.

Recently, significant progress in symmetry-based strategies [33–38] greatly accelerates the discovery of both topological insulating states and topological semimetals [39–41]. However, these elegant strategies can lead to “false-negative” results in identifying Weyl semimetals [42,43]. Because of the inexistence of a suitable topological invariant characterizing the Weyl semimetals, the search of them is comparatively difficult. Surprisingly, there is a special system, i.e., magnetic centrosymmetric system, for which the topological invariant χ can be defined by

$$(-1)^{\chi} \equiv \prod_{j=\{1,2,\ldots,n_{occ}\},\Gamma_i=\text{TRIMs}} \xi_i^j, \qquad (1)$$

where ξ_i^j is the parity eigenvalue (± 1) of the jth band at the time-reversal-invariant-momentum (TRIM) Γ_i, and n_{occ} is the total number of the valence bands. If $\chi = 1$, the system must have band crossing points around the Fermi level, and may be a Weyl semimetal [44–46]. Although the hydrogen atom of nonmagnetic Weyl semimetal has been discovered [47], and there are some high-throughput screening methods for Weyl semimetals [43,48–50], the discovery of the hydrogen atom of magnetic Weyl semimetals is still challenging but represents a highly desirable state.

In this Letter, the topological properties of alluaudite-type compound $K_2Mn_3(AsO_4)_3$ are systematically studied based on first-principles calculations and low-energy effective model analysis. The total energy calculations show that $K_2Mn_3(AsO_4)_3$ favors a ferromagnetic (FM) ground state with magnetic momentum in the z direction (i.e., $[\bar{1}01]$ direction). The FM $K_2Mn_3(AsO_4)_3$ hosts only a pair of WPs with opposite chirality around the Z point, which are constrained in the z direction by the twofold rotation symmetry around the direction. More interestingly, extremely long Fermi arcs exist on the yoz plane of $K_2Mn_3(AsO_4)_3$, which can be easily observed by an angle-resolved photoemission spectroscopy experiment. Based on its low-energy effective model, the possible nontrivial superconductor (SC) states are explored, which gives rise to the discovery of various novel states, such as the hydrogen atom of Weyl SC. The hydrogen atom of FM Weyl semimetal in $K_2Mn_3(AsO_4)_3$ greatly facilitates the study of Weyl-related physics only and the device applications of Weyl semimetals.

Crystal and magnetic structures of $K_2Mn_3(AsO_4)_3$.—$K_2Mn_3(AsO_4)_3$ has been experimentally fabricated in bulk since 2012 [51]. The crystal structure was identified to be of the alluaudite-type which can be described by the formula $A(2)A(1)M(1)M(2)_2(XO_4)_3$ [52]. This structure contains two sets of tunnels in the [010] direction with A atoms at the centers, embedded in the $M(1)M(2)_2(XO_4)_3$ framework (see details in Sec. B of the Supplemental Material [53]). The framework is formed by chains of edge-sharing MO_6 octahedra, which are linked together by the XO_4 tetrahedra. The remarkable flexibility of the framework allows cation substitution in the X and M sites and tolerates a wide range of compositional variations, leading to the presence of interesting electrical transport and magnetic properties [64–68]. Given the partial occupation of Mn d orbitals and the observation of magnetic property in alluaudite-type manganese sulphate [67], we anticipate a possible magnetic ground state in $K_2Mn_3(AsO_4)_3$. By using the generalized gradient approximation (GGA) + Hubbard-U (GGA + U) method, the possible magnetic structures of $K_2Mn_3(AsO_4)_3$ have been explored (see calculation method in Sec. A of the Supplemental Material [53]). Here, we studied eleven collinear magnetic configurations, including ten antiferromagnetic (AFM)-like configurations and one FM configuration. The calculations show that the total energy of the nonmagnetic state is about 45 eV/unit cell lower than that of the magnetic states. Moreover, the FM configuration lowers the total energy by dozens of meV compared to AFM-like configurations, and is the ground state of $K_2Mn_3(AsO_4)_3$ (see details in Sec. C of the Supplemental Material [53]).

Band structures of $K_2Mn_3(AsO_4)_3$.—Based on the FM structure, the band structures of $K_2Mn_3(AsO_4)_3$ are calculated and shown in Fig. 1. In the GGA + U band structure without the consideration of spin-orbit coupling (SOC), there is a band inversion between the Γ_1^+ band and the Γ_2^- band at the Z point, which gives rise to a nodal line circled around the point, as shown in Figs. 1(b) and 1(d). The nodal line is protected by the coexistence of inversion symmetry and time reversal symmetry (TRS). When SOC is included, the overall shape of the band structure around the Fermi level (E_F) changes very little except the band gap opening at the nodal line [Fig. 1(c)]. As the system still has the inversion symmetry, and the irreducible representations of the two inverted bands become Γ_3^+ and Γ_4^-, respectively, the topological invariant χ in Eq. (1) is well defined. According to the numbers of even and odd valence bands at eight TRIMs in Table I, χ is computed to be 1, guaranteeing the presence of band crossing points around the Fermi level. Our calculations show that band gaps open up along the nodal line except two gapless points (i.e., WPs) on the k_z axis, as shown in Figs. 1(c) and 1(e). The WPs with opposite chirality [Fig. 1(f)] are constrained on the k_z axis due to the twofold rotation symmetry $\{\hat{C}_2^z|0,\frac{1}{2},0\}$.

Topological surface states and Fermi arcs.—In view of the fact that one hallmark of Weyl semimetal is the existence of Fermi-arc surface states, maximally localized Wannier functions (MLWFs) for the d orbitals of Mn and p orbitals of O are constructed, which are used to build the Green's functions of the semi-infinite slabs by using an iterative method. The local density of states (LDOS) on yoz surface, extracted from the imaginary parts of the surface

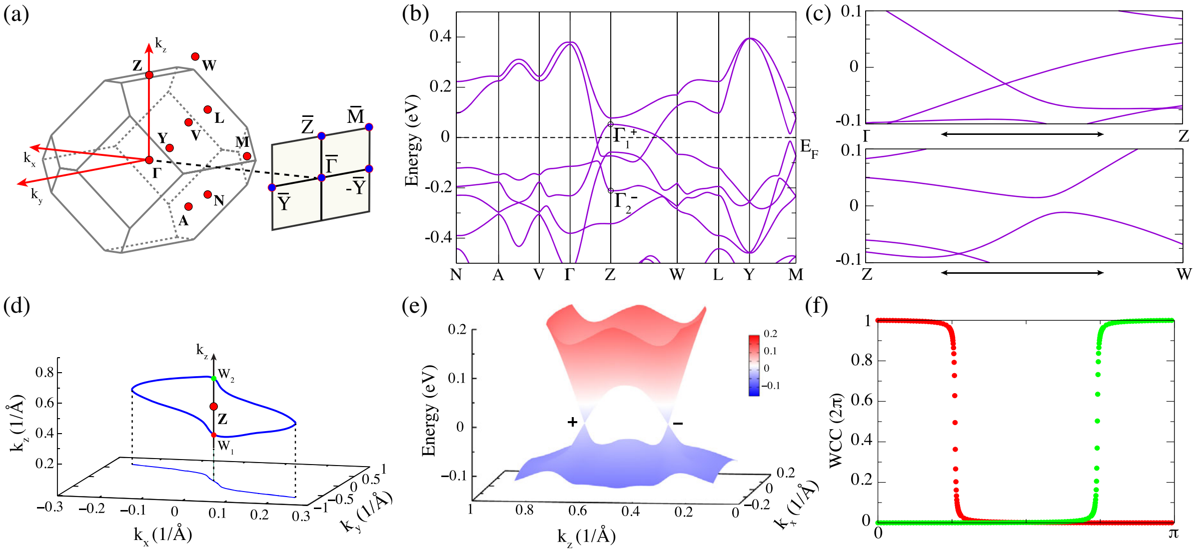

FIG. 1. Electronic structure of $K_2Mn_3(AsO_4)_3$. (a) The bulk BZ and the projected yoz-surface BZ with high-symmetry points. (b) The GGA + U band structure of $K_2Mn_3(AsO_4)_3$. (c) The GGA + U + SOC band structure around the band crossing points near the Fermi level. (d) The nodal line around the Z point in the BZ. (e) Three-dimensional band structure around the WPs. (f) The evolution of Wannier charge centers (WCCs) on two spheres enclosing W_1 (red dots) and W_2 (green dots), respectively. The coordinates of W_1 and W_2 are $\vec{K}^Z \mp (0,0,0.156621)$ in units of 1/Å, respectively.

TABLE I. The numbers of even and odd valence bands at eight TRIMs. The positions of the TRIMs are given in three primitive reciprocal vectors.

TRIM	Position	Even parity	Odd parity
Γ	(0,0,0)	122	130
Y	(0,0.5,0)	126	126
Z	(−0.5, 0, 0.5)	121	131
A	(0.5,0,0)	130	122
V	(0,0,0.5)	130	122
L	(0,0.5,0.5)	126	126
N	(0.5,0.5,0)	126	126
M	(0.5,0.5,0.5)	126	126

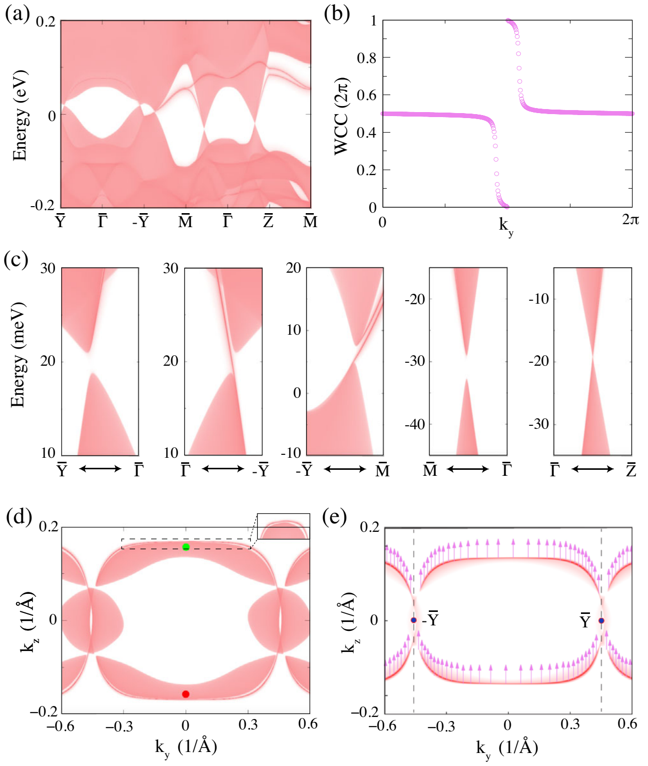

FIG. 2. Surface states and Fermi arcs. (a),(c) Energy and momentum dependence of the LDOS on *yoz* surface for $K_2Mn_3(AsO_4)_3$. (b) The evolution of WCCs as a function of k_y for the $k_z = 0$ plane. (d) Fermi-arc surface states on *yoz* surface at Fermi level. The projected WPs are shown as red and green dots for different chirality. It is worth noting that the surface projection of the Z point is the same as the $\bar{\Gamma}$ point as they differ by a primitive reciprocal vector of the surface BZ (see the definitions of the surface primitive reciprocal vectors in Supplemental Material [53]). So, the projected WPs shown as red and green dots for different chirality are located at $(k_y, k_z) = (0, \mp 0.156621)$ in units of $1/\text{Å}$. (e) Same as (d) but with the Fermi arc states at Fermi level highlighted. The spin texture of the Fermi arc states are represented by arrows.

Green's functions, are shown in Fig. 2. On the *yoz* surface, the WPs are projected to the $\bar{\Gamma}$-$\bar{Z}$ direction, leading to the existence of gapless dispersion in the direction, as shown in Figs. 2(a) and 2(c). Along the $\bar{\text{Y}}$-$\bar{\Gamma}$-$(-\bar{\text{Y}})$ line, there is one surface state crossing the Fermi level, which is consistent with the nontrivial Chern number (i.e., $C = -1$) of the $k_z = 0$ plane, as shown in Figs. 2(b) and 2(c). In addition, the constant-energy contour of the surface states clearly shows that two Fermi-arc surface states derived from two bulk electron pockets in the $(-\bar{Z})$-$\bar{\Gamma}$-$\bar{Z}$ direction (enclosing two opposite-chirality WPs, respectively) are buried in the same bulk hole pocket in the $\bar{\text{Y}}$-$\bar{\Gamma}$-$(-\bar{\text{Y}})$ direction, as shown in Figs. 2(d) and 2(e). Because the Fermi arc surface states are slightly buried in the bulk states at Fermi level, the Fermi arc states around $\bar{\text{Y}}$ or $-\bar{\text{Y}}$ are blurred. However, a Fermi arc line crossing the $k_z = 0$ line can still be seen. Compared with Fermi-arc surface states in well-known nonmagnetic Weyl semimetals (such as TaAs [8]), there are two distinct features of the Fermi arcs in $K_2Mn_3(AsO_4)_3$: (i) the Fermi arcs are extremely long, which are desirable to the related device applications; (ii) the two states at $\bar{k}$ and $-\bar{k}$ on the constant-energy contour carry parallel spin alignment.

Low-energy effective model.—In order to understand the main feature of the low-energy band structure of $K_2Mn_3(AsO_4)_3$, an effective low-energy 2×2 $k \cdot p$ model is constructed (see details in Sec. D of the Supplemental Material [53]). When SOC is ignored and the constraints placed by all symmetries [including inversion symmetry $\hat{I}$, glide mirror symmetry $\hat{g}_z = \{\hat{M}_z | 0, \frac{1}{2}, 0\}$ (the translation is given in units of three primitive lattice vectors) and TRS $\mathcal{T}$] are considered, the model with the Γ_1^+ band and the Γ_2^- band as the basis can be up to second order of $\mathbf{k}$ written as

$$H^Z(\mathbf{k}) = d_y(\mathbf{k})\sigma_y + d_z(\mathbf{k})\sigma_z,$$
$$\text{with} \quad \mathbf{k} \equiv (k_x, k_y, k_z) = (K_x, K_y, K_z) - \vec{K}^Z, \qquad (2)$$

where $\mathbf{k}$ is the momentum vector relative to the Z point; $\sigma_{y,z}$ are Pauli matrices. $d_y(\mathbf{k})$ and $d_z(\mathbf{k})$ are odd and even real functions of $\mathbf{k}$, respectively. The eigenvalues of Eq. (2) are $E(\mathbf{k}) = \pm\sqrt{d_y^2(\mathbf{k}) + d_z^2(\mathbf{k})}$. The degenerate band crossings require

$$d_y(\mathbf{k}) = b_2 k_x + b_3 k_y = 0, \qquad (3)$$

$$d_z(\mathbf{k}) = c_1 + c_4 k_x^2 + c_5 k_y^2 + c_6 k_z^2 + c_7 k_x k_y = 0. \qquad (4)$$

By substituting Eq. (3) into Eq. (4), it is easy to get the following equality:

$$-\frac{(b_3^2 c_4 + b_2^2 c_5 - b_2 b_3 c_7)}{b_2^2 c_1} k_y^2 - \frac{c_6}{c_1} k_z^2 = 1. \qquad (5)$$

As the two bands are inverted along the Γ-Z direction, we can get the requirement $c_1 c_6 < 0$. Therefore, the

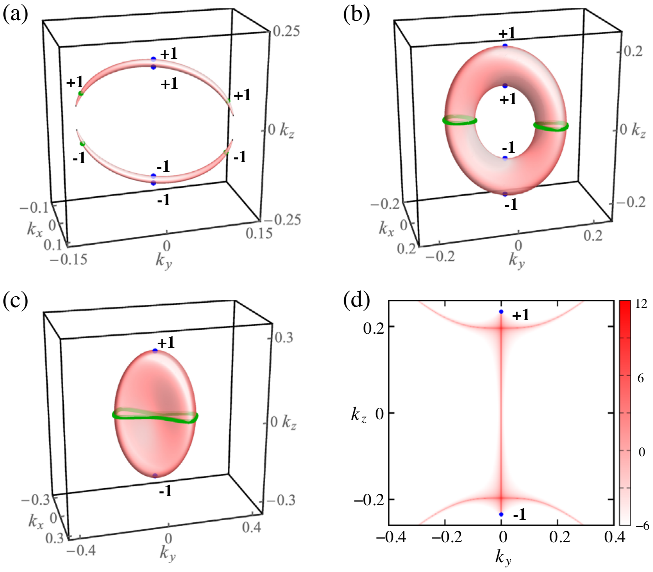

FIG. 3. The FS and the superconducting gap structure. The crescent (a), torus (b), and ellipsoidlike (c) FS of $K_2Mn_3(AsO_4)_3$ with chemical potential at $\mu = 0.01$, 0.05, and 0.1 eV, respectively. The gapless structures of the pairing potential Δ_{A_u} (green dots or lines) and Δ_{B_u} (blue dots). (d) The crossed surface Andreev bound states in the B_u state with $\mu = 0.1$ eV. The Z or $\bar{Z}$ point is chosen as the origin point. The charges of the WPs are indicated.

prefactor of k_z^2 (i.e., $-c_6/c_1$) is greater than 0, and the Eq. (5) is a hyperbola or an ellipse depending on the sign of the prefactor of k_y^2. By fitting the first-principles band structure with the model, the values of these parameters are obtained, as shown in Table S4 [53]. It is easy to find the sign of the prefactor of k_y^2 is plus. Therefore, the analysis of the model shows that the band crossing points around the Fermi level in $K_2Mn_3(AsO_4)_3$ form an ellipse around the Z point, which is consistent with our first-principles calculations.

After the consideration of SOC, the TRS is broken, while the glide mirror symmetry and inversion symmetry are preserved. Therefore, it is easy to get the effective model with SOC, as shown below

$$H^Z_{\mathrm{SOC}}(\mathbf{k}) = d_x(\mathbf{k})\sigma_x + d_y(\mathbf{k})\sigma_y + d_z(\mathbf{k})\sigma_z, \qquad (6)$$

where $d_x(\mathbf{k})$ is an odd real function of $\mathbf{k}$ (see details in Sec. D of the Supplemental Material [53]). The eigenvalues of Eq. (6) are $E(\mathbf{k}) = \pm\sqrt{d_x^2(\mathbf{k}) + d_y^2(\mathbf{k}) + d_z^2(\mathbf{k})}$. The degenerate band crossings require $d_x(\mathbf{k}) = d_y(\mathbf{k}) = d_z(\mathbf{k}) = 0$. Because $c_1c_6 < 0$, there are two gapless points at $(0, 0, \pm\sqrt{-c_1/c_6})$, which are WPs in the $(-Z)$-Γ-Z direction. Therefore, the $k \cdot p$ models can capture the low-energy physics in $K_2Mn_3(AsO_4)_3$.

The nontrivial SC states.—Weyl semimetals without TRS are considered as a promising platform to realize the nontrivial SC states with Majorana quasiparticles [69]. This is because, in the presence of the inversion symmetry but absence of the TRS, the spin configuration of the Cooper pair is parallel, namely, conventional spin-singlet s-wave state is excluded from the candidate of the pairing symmetry. Next, we briefly discuss the possible SC state in $K_2Mn_3(AsO_4)_3$ using the $k \cdot p$ model derived above. The remarkable feature of $K_2Mn_3(AsO_4)_3$ is that the shape of the Fermi surface (FS) can be easily tuned by doping as its structure allows a wide range of cationic substitution in K and Mn sites. We hence also clarify how the SC properties develop according to the evolution of the FS.

To describe the SC state, we start from the mean-field Hamiltonian in the Bogoliubov–de Gennes (BdG) formalism:

$$H_{\mathrm{BdG}} = \int d\mathbf{k}\boldsymbol{c}^\dagger_{\mathbf{k}} H(\mathbf{k})\boldsymbol{c}_{\mathbf{k}}, \qquad (7)$$

$$H(\mathbf{k}) = \begin{pmatrix} H^Z_{SOC}(\mathbf{k}) - \mu & \Delta(\mathbf{k}) \\ \Delta^\dagger(\mathbf{k}) & -H^{Z*}_{SOC}(-\mathbf{k}) + \mu \end{pmatrix}, \qquad (8)$$

$$\boldsymbol{c}_{\mathbf{k}} = (c_{1,\mathbf{k}}, c_{2,\mathbf{k}}, c^\dagger_{1,-\mathbf{k}}, c^\dagger_{2,-\mathbf{k}}), \qquad (9)$$

where $\Delta(\mathbf{k})$ is the SC pairing potential and μ is the chemical potential. For the above BdG Hamiltonian, we consider the following pairing potentials which can be classified into four irreducible representations of the $\mathcal{C}_{2h}$ point group: $\Delta_{A_g} \equiv i\Delta_0 k_x\sigma_x$, $\Delta_{B_g} \equiv i\Delta_0 k_z\sigma_x$, $\Delta_{A_u} \equiv i\Delta_0 k_z\sigma_0$, and $\Delta_{B_u} \equiv i\Delta_0\sigma_y$. To clearly see the SC gap structure of each pairing state, we derive the single band representation of the pairing potential (see details in Sec. E of the Supplemental Material [53]).

TABLE II. SC gap structures and the type of SC of the possible pairing states. The number and position of the gapless structure are shown in brackets.

Representation	Crescent FS	Torus or ellipsoid FS	Type of SC
Δ_{A_g}	Nodal surface	Nodal surface	Gapless
Δ_{B_g}	Nodal surface	Nodal surface	Gapless
Δ_{A_u}	WPs (4, generic)	Nodal line (2 or 1, $k_z = 0$ plane)	p_z + chiral-f
Δ_{B_u}	WPs (4, k_z axis)	WPs (4 or 2, k_z axis)	Chiral-p

It is found that the conduction band components of the even-parity pairings, Δ_{A_g} and Δ_{B_g}, are zero, which means that they have similar nodal surfaces (i.e., crescent, torus, and ellipsoidlike nodal surfaces). Interestingly, the crescent nodal surface states are topologically protected and characterized by a pair of topological charges (i.e., $\mathbb{Z}_2 \oplus 2\mathbb{Z}$) (see details in Sec. F of the Supplemental Material [53]) [70,71]. However, the even-parity pairing states are less likely to occur due to the inexistence of the superconducting gap. On the other hand, for the odd-parity pairings, the single band representations are obtained as

$$\tilde{\Delta}^c_{A_u} = \frac{ik_z\Delta_0}{2}\left[1 + \frac{d_z(\mathbf{k})}{\varepsilon} - \left(1 - \frac{d_z(\mathbf{k})}{\varepsilon}\right)e^{-2i\theta}\right], \qquad (10)$$

$$\tilde{\Delta}^c_{B_u} = -\frac{\Delta_0}{\varepsilon}[d_x(\mathbf{k}) - id_y(\mathbf{k})], \qquad (11)$$

indicating that Δ_{A_u} and Δ_{B_u} can be effectively considered as $p_z +$ chiral f-wave state and chiral p-wave state, respectively. By solving $\tilde{\Delta}^c_\alpha = 0$ ($\alpha = A_u$ or B_u), it is found that Δ_{A_u} and Δ_{B_u} pairings exhibit WPs or nodal lines depending on the position of the chemical potential μ, as shown in Fig. 3. When the FS is the crescent shape ($\mu = 0.01$ eV), WPs on the generic momenta and k_z axis are presented in the Δ_{A_u} and Δ_{B_u} pairings, respectively. On the other hand, when the FS is a torus ($\mu = 0.05$ eV) or an ellipsoidlike ($\mu = 0.1$ eV) surface, the nodal lines (WPs) appear on the $k_z = 0$ plane (k_z axis) for the Δ_{A_u} (Δ_{B_u}) pairing. The SC gap structures of the possible pairing states are also summarized in Table II. When the chemical potential is low, there are two pairs of WPs on the k_z axis for the B_u state. As the chemical potential increases, one of the pairs approach each other. They meet and annihilate at the BZ's center finally (see details in Sec. F of the Supplemental Material [53]). Therefore, there is only a pair of WPs left, i.e., it is a hydrogen atom of Weyl SC. The WPs lead to novel crossed surface Andreev bound states, which are associated with the nontrivial Chern number [72], as shown in Fig. 3(d).

Conclusion.—In summary, we propose that hydrogen atom of magnetic Weyl semimetal can be realized in the FM alluaudite-type compound $K_2Mn_3(AsO_4)_3$. The presence of two WPs constrained in the z direction leads to extremely long Fermi arcs on the yoz plane, which are expected to be easily observed in measurements. Moreover, we have shown that the odd-parity chiral p-wave and chiral f-wave state can be realized in $K_2Mn_3(AsO_4)_3$. Depending on the shape of the FS, a wide variety of the superconducting gap structure can be realized in the odd-parity SC, such as hydrogen atom of Weyl SC with novel crossed surface Andreev bound states.

This work was supported by the Affiliates Program of the Nanoscale Prototyping Laboratory at Stanford University

---

[*] smnie@stanford.edu

[†] S. N. and T. H. contributed equally to this work.

[‡] fprinz@stanford.edu

[1] Z. Wang, Y. Sun, X.-Q. Chen, C. Franchini, G. Xu, H. Weng, X. Dai, and Z. Fang, Phys. Rev. B **85**, 195320 (2012).
[2] Z. Wang, H. Weng, Q. Wu, X. Dai, and Z. Fang, Phys. Rev. B **88**, 125427 (2013).
[3] S. Murakami, New J. Phys. **9**, 356 (2007).
[4] X. Wan, A. M. Turner, A. Vishwanath, and S. Y. Savrasov, Phys. Rev. B **83**, 205101 (2011).
[5] A. A. Burkov and L. Balents, Phys. Rev. Lett. **107**, 127205 (2011).
[6] G. Xu, H. Weng, Z. Wang, X. Dai, and Z. Fang, Phys. Rev. Lett. **107**, 186806 (2011).
[7] J. Liu and D. Vanderbilt, Phys. Rev. B **90**, 155316 (2014).
[8] H. Weng, C. Fang, Z. Fang, B. A. Bernevig, and X. Dai, Phys. Rev. X **5**, 011029 (2015).
[9] A. Burkov, Nat. Mater. **15**, 1145 (2016).
[10] S. Nie, G. Xu, F. B. Prinz, and S.-c. Zhang, Proc. Natl. Acad. Sci. U.S.A. **114**, 10596 (2017).
[11] B. Yan and C. Felser, Annu. Rev. Condens. Matter Phys. **8**, 337 (2017).
[12] D. F. Liu, A. J. Liang, E. K. Liu, Q. N. Xu, Y. W. Li, C. Chen, D. Pei, W. J. Shi, S. K. Mo, P. Dudin *et al.*, Science **365**, 1282 (2019).
[13] I. Belopolski, K. Manna, D. S. Sanchez, G. Chang, B. Ernst, J. Yin, S. S. Zhang, T. Cochran, N. Shumiya, H. Zheng *et al.*, Science **365**, 1278 (2019).
[14] N. Morali, R. Batabyal, P. K. Nag, E. Liu, Q. Xu, Y. Sun, B. Yan, C. Felser, N. Avraham, and H. Beidenkopf, Science **365**, 1286 (2019).
[15] M. Sato and Y. Ando, Rep. Prog. Phys. **80**, 076501 (2017).
[16] N. P. Armitage, E. J. Mele, and A. Vishwanath, Rev. Mod. Phys. **90**, 015001 (2018).
[17] B. Q. Lv, T. Qian, and H. Ding, Rev. Mod. Phys. **93**, 025002 (2021).
[18] P. Zhang, K. Yaji, T. Hashimoto, Y. Ota, T. Kondo, K. Okazaki, Z. Wang, J. Wen, G. Gu, H. Ding, and S. Shin, Science **360**, 182 (2018).
[19] S. Nadj-Perge, I. K. Drozdov, J. Li, H. Chen, S. Jeon, J. Seo, A. H. MacDonald, B. A. Bernevig, and A. Yazdani, Science **346**, 602 (2014).
[20] D. Wang, L. Kong, P. Fan, H. Chen, S. Zhu, W. Liu, L. Cao, Y. Sun, S. Du, J. Schneeloch *et al.*, Science **362**, 333 (2018).
[21] S. Nie, L. Xing, R. Jin, W. Xie, Z. Wang, and F. B. Prinz, Phys. Rev. B **98**, 125143 (2018).
[22] H. Weyl, Z. Phys. **56**, 330 (1929).
[23] Z. Fang, N. Nagaosa, K. S. Takahashi, A. Asamitsu, R. Mathieu, T. Ogasawara, H. Yamada, M. Kawasaki, Y. Tokura, and K. Terakura, Science **302**, 92 (2003).
[24] H. B. Nielsen and M. Ninomiya, Phys. Lett. **130B**, 389 (1983).
[25] B. A. Bernevig, Nat. Phys. **11**, 698 (2015).

[26] X. Huang, L. Zhao, Y. Long, P. Wang, D. Chen, Z. Yang, H. Liang, M. Xue, H. Weng, Z. Fang, X. Dai, and G. Chen, Phys. Rev. X **5**, 031023 (2015).

[27] D. T. Son and B. Z. Spivak, Phys. Rev. B **88**, 104412 (2013).

[28] F. Arnold, C. Shekhar, S.-C. Wu, Y. Sun, R. D. Dos Reis, N. Kumar, M. Naumann, M. O. Ajeesh, M. Schmidt, A. G. Grushin *et al.*, Nat. Commun. **7**, 11615 (2016).

[29] A. A. Burkov, Phys. Rev. Lett. **113**, 187202 (2014).

[30] H. Weng, R. Yu, X. Hu, X. Dai, and Z. Fang, Adv. Phys. **64**, 227 (2015).

[31] E. Liu, Y. Sun, N. Kumar, L. Muechler, A. Sun, L. Jiao, S.-Y. Yang, D. Liu, A. Liang, Q. Xu *et al.*, Nat. Phys. **14**, 1125 (2018).

[32] Q. Wang, Y. Xu, R. Lou, Z. Liu, M. Li, Y. Huang, D. Shen, H. Weng, S. Wang, and H. Lei, Nat. Commun. **9**, 3681 (2018).

[33] H. C. Po, A. Vishwanath, and H. Watanabe, Nat. Commun. **8**, 50 (2017).

[34] B. Bradlyn, L. Elcoro, J. Cano, M. Vergniory, Z. Wang, C. Felser, M. Aroyo, and B. A. Bernevig, Nature (London) **547**, 298 (2017).

[35] E. Khalaf, H. C. Po, A. Vishwanath, and H. Watanabe, Phys. Rev. X **8**, 031070 (2018).

[36] J. Kruthoff, J. de Boer, J. Van Wezel, C. L. Kane, and R.-J. Slager, Phys. Rev. X **7**, 041069 (2017).

[37] Z. Song, T. Zhang, Z. Fang, and C. Fang, Nat. Commun. **9**, 3530 (2018).

[38] F. Tang, H. C. Po, A. Vishwanath, and X. Wan, Nat. Phys. **15**, 470 (2019).

[39] M. Vergniory, L. Elcoro, C. Felser, N. Regnault, B. A. Bernevig, and Z. Wang, Nature (London) **566**, 480 (2019).

[40] F. Tang, H. C. Po, A. Vishwanath, and X. Wan, Nature (London) **566**, 486 (2019).

[41] T. Zhang, Y. Jiang, Z. Song, H. Huang, Y. He, Z. Fang, H. Weng, and C. Fang, Nature (London) **566**, 475 (2019).

[42] Y. Qian, J. Gao, Z. Song, S. Nie, Z. Wang, H. Weng, and Z. Fang, Phys. Rev. B **101**, 155143 (2020).

[43] J. Gao, Y. Qian, S. Nie, Z. Fang, H. Weng, and Z. Wang, Sci. Bull. **66**, 667 (2021).

[44] Z. Wang, M. G. Vergniory, S. Kushwaha, M. Hirschberger, E. V. Chulkov, A. Ernst, N. P. Ong, R. J. Cava, and B. A. Bernevig, Phys. Rev. Lett. **117**, 236401 (2016).

[45] T. L. Hughes, E. Prodan, and B. A. Bernevig, Phys. Rev. B **83**, 245132 (2011).

[46] S. Nie, Y. Sun, F. B. Prinz, Z. Wang, H. Weng, Z. Fang, and X. Dai, Phys. Rev. Lett. **124**, 076403 (2020).

[47] I. Belopolski, P. Yu, D. S. Sanchez, Y. Ishida, T.-R. Chang, S. S. Zhang, S.-Y. Xu, H. Zheng, G. Chang, G. Bian *et al.*, Nat. Commun. **8**, 942 (2017).

[48] V. Ivanov and S. Y. Savrasov, Phys. Rev. B **99**, 125124 (2019).

[49] Y. Xu, L. Elcoro, Z.-D. Song, B. J. Wieder, M. Vergniory, N. Regnault, Y. Chen, C. Felser, and B. A. Bernevig, Nature (London) **586**, 702 (2020).

[50] Q. Xu, Y. Zhang, K. Koepernik, W. Shi, J. van den Brink, C. Felser, and Y. Sun, npj Comput. Mater. **6**, 32 (2020).

[51] S. Chaalia, B. Ayed, and A. Haddad, Journal of Chemical Crystallography **42**, 941 (2012).

[52] P. B. Moore, Am. Mineral. **56**, 1955 (1971), https://pubs.geoscienceworld.org/msa/ammin/article-pdf/56/11-12/1955/4250838/am-1971-1955.pdf.

[53] See Supplemental Material at http://link.aps.org/supplemental/10.1103/PhysRevLett.128.176401 for the details on the calculation method, the lattice and crystal symmetries, the total energies of collinear magnetic structures, the $k \cdot p$ models, topological superconducting states, and the stability and topological properties of the gapless states, which includes Refs. [54–63].

[54] G. Kresse and J. Furthmüller, Comput. Mater. Sci. **6**, 15 (1996).

[55] G. Kresse and J. Furthmüller, Phys. Rev. B **54**, 11169 (1996).

[56] J. P. Perdew, K. Burke, and M. Ernzerhof, Phys. Rev. Lett. **77**, 3865 (1996).

[57] A. I. Liechtenstein, V. I. Anisimov, and J. Zaanen, Phys. Rev. B **52**, R5467 (1995).

[58] N. Marzari and D. Vanderbilt, Phys. Rev. B **56**, 12847 (1997).

[59] I. Souza, N. Marzari, and D. Vanderbilt, Phys. Rev. B **65**, 035109 (2001).

[60] N. Marzari, A. A. Mostofi, J. R. Yates, I. Souza, and D. Vanderbilt, Rev. Mod. Phys. **84**, 1419 (2012).

[61] M. L. Sancho, J. L. Sancho, and J. Rubio, J. Phys. F **14**, 1205 (1984).

[62] M. L. Sancho, J. L. Sancho, J. L. Sancho, and J. Rubio, J. Phys. F **15**, 851 (1985).

[63] R. Nandkishore, Phys. Rev. B **93**, 020506(R) (2016).

[64] J. Kim, H. Kim, S. Lee, and S.-T. Myung, J. Mater. Chem. A **5**, 22334 (2017).

[65] C. Karegeya, A. Mahmoud, B. Vertruyen, F. Hatert, R. P. Hermann, R. Cloots, and F. Boschini, J. Solid State Chem. **253**, 389 (2017).

[66] N. Chouaibi, A. Daidouh, C. Pico, A. Santrich, and M. Veiga, J. Solid State Chem. **159**, 46 (2001).

[67] D. Dwibedi, R. B. Araujo, S. Chakraborty, P. P. Shanbogh, N. G. Sundaram, R. Ahuja, and P. Barpanda, J. Mater. Chem. A **3**, 18564 (2015).

[68] R. Essehli, B. El Bali, S. Benmokhtar, K. Bouziane, B. Manoun, M. A. Abdalslam, and H. Ehrenberg, J. Alloys Compd. **509**, 1163 (2011).

[69] M. Sato and Y. Ando, Rep. Prog. Phys. **80**, 076501 (2017).

[70] D. F. Agterberg, P. M. R. Brydon, and C. Timm, Phys. Rev. Lett. **118**, 127001 (2017).

[71] T. c. v. Bzdušek and M. Sigrist, Phys. Rev. B **96**, 155105 (2017).

[72] B. Lu, K. Yada, M. Sato, and Y. Tanaka, Phys. Rev. Lett. **114**, 096804 (2015).